

Fluorescence Imaging Micro-Spectrophotometer (FIMS)

Douglas C. Youvan, William J. Coleman, Chris M. Silva, Julien Petersen,
Edward J. Bylina, and Mary M. Yang*

*Corresponding Author:

KAIROS Scientific Inc.
Bldg. 62
3350 Scott Blvd.
Santa Clara, CA 95054 USA

E-mail: myang@kairos-scientific.com

Website: www.kairos-scientific.com

Received: N/A

Accepted: N/A

Abstract

A prototype spectrophotometer is described which combines the *spatial* resolution of an epifluorescence microscope ($<1\ \mu\text{m}$) with the *spectral* resolution of a conventional fluorimeter ($\sim 2\ \text{nm}$). This *Fluorescence Imaging MicroSpectrophotometer* (FIMS) acquires fluorescence excitation or emission stacks within minutes and then rapidly compresses the data into a pseudocolored image, wherein each color represents a different spectral category. FIMS technology replaces the fixed-wavelength excitation and emission filters of a conventional epifluorescence microscope with fully tunable wavelength selection, thus allowing the fluorescence spectrum of every pixel in a scene to be simultaneously determined. Hyperspectral pseudocoloring software has been written which reduces these image stacks into a single image, while maintaining the radiometric calibration of each pixel's spectrum and providing overall spectral statistics on each pseudocolored category. Categories are determined by rapid processing of all the pixels within a scene according to a variety of sorting algorithms which group together pixels exhibiting similar spectra. FIMS data acquisition and processing are demonstrated on spectral stacks containing data from: (1) six different fluorescent microspheres emitting between 520 and 720 nm, and (2) bacteria expressing various forms of the Green Fluorescent Protein (i.e., wild-type and variants with red-shifted excitation and red-shifted emission) excited between 355 and 505 nm.

Introduction

Imaging Spectroscopy. Imaging spectroscopy is defined as the combined analysis of both spatial and spectral information. In terms of *absorption* spectra, 'image stacks' have been described in which each 2-dimensional image in the stack displays how the target would appear if illuminated by monochromatic light of a particular wavelength (Vane *et al.*, 1993; Youvan, 1994; Youvan *et al.*, 1994; Yang *et al.*, 1996; Wang & Herman, 1996). Previously, we have described imaging spectrophotometers for making absorption measurements on macroscopic targets such as bacterial colonies on petri dishes (Youvan, 1994); in a future publication, we will describe the acquisition and processing of absorbance data from a high-power brightfield microscope. In the present paper, we apply this technology to *fluorescence* spectroscopy, by developing and demonstrating a prototype *Fluorescence Imaging MicroSpectrophotometer* (FIMS).

As in a conventional fluorimeter, FIMS acquires fluorescence data according to various excitation and emission scanning parameters. By setting a blocking filter to a constant wavelength, excitation stacks can be obtained by scanning from shorter wavelengths up to the emission wavelength. Similarly, emission stacks can be generated by setting the excitation to a constant wavelength and tuning the blocking filter, while capturing a series of images to the red of the exciting light. This has a direct parallel in conventional fluorimetry and micro-spectrofluorimetry (Ruch & Leemann, 1973; Hirschberg *et al.*, 1979; Kohen *et al.*, 1981; Kasten, 1989), and a corresponding complexity with regard to the number of different ways that the excitation and/or emission scans can be performed to acquire various datasets. But whereas other fluorescence microscopes typically scan the image at a given wavelength (Ploem, 1989; Arndt-Jovin & Jovin, 1989), FIMS acquires data on all of the pixels at a given wavelength simultaneously.

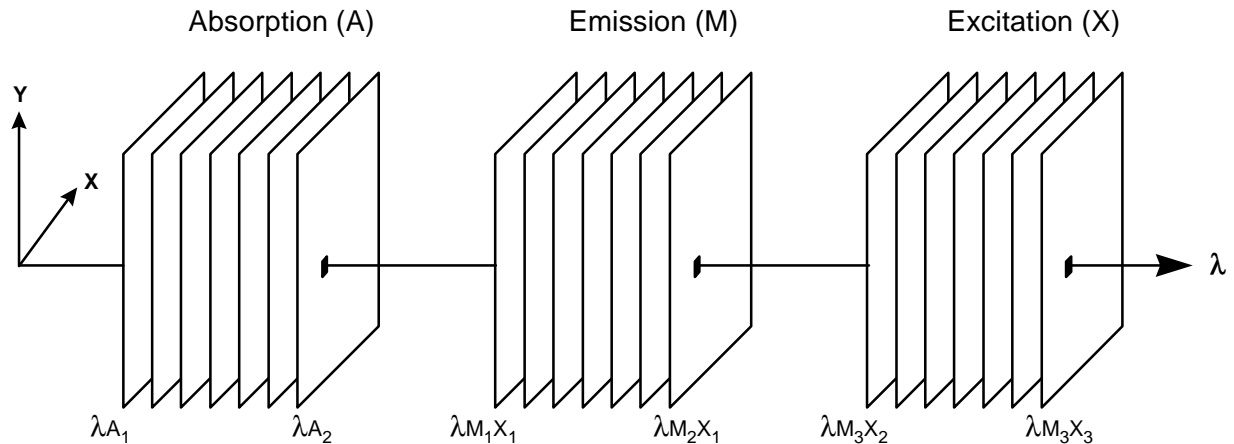


Fig. 1. Schematic representation of image stacks acquired by the FIMS instrument. Image stacks are intrinsically 3-dimensional, with two spatial dimensions (x, y) that form the image plane and a third dimension (λ) that represents the spectrum of each pixel. As depicted in the figure, stacks generated from different spectroscopic measurements can be spatially co-registered; thus, absorption, fluorescence emission, and fluorescence excitation spectra can be recalled for any pixel in a scene as illustrated by the horizontal arrow. Modes: **A**bsorption, A; **E**xcitation, X; **E**mission, M. Starting and ending wavelengths for: absorption, A_1 and A_2 ; emission M_1 and M_2 ; excitation X_2 and X_3 , respectively, at the fixed wavelengths for excitation X_1 and emission M_3 .

FIMS is capable of imaging samples which utilize either organic fluorophores or newly discovered fluorescent proteins as markers. In either case, the instrument operates in a massively parallel manner by essentially enabling every pixel in the CCD camera to function as a spectrofluorimeter. This means that a full excitation or emission spectrum can be acquired for every pixel in a scene, which then allows the software to process images using parameters derived from continuous (i.e., spectrophotometer-quality) data. This feature is especially important for targets which contain multiple fluorophores that might overlap in either the spatial or spectral dimension.

Green Fluorescent Protein. A multitude of recent experiments have used the Green Fluorescent Protein (GFP) to study gene expression, protein trafficking, and protein-protein interactions (Chalfie *et al.*, 1994; Delagrave *et al.*, 1995; Doyle & Botstein, 1996; Yokoe & Meyer, 1996; Htun *et al.*, 1996; Plautz *et al.*, 1996). GFP chimeras with blue or green fluorescence emission have enabled cell biologists to monitor proteins *in vivo* without exogenously added dyes. One of the simplest applications of FIMS in cell biology is to accurately and quantitatively analyze samples in which two or more such fluorescent labels are present. This problem is more difficult than it seems, because determining the percentage of each derivative (e.g., blue or green) in a 'mixed pixel' requires full spectral deconvolution. This arises from the fact that the spectra of the fluorophores usually overlap. The most common manifestation of this phenomenon occurs in samples containing both blue and green GFP derivatives, which might be categorized, in a simplistic manner, as fluorescing in the blue and green channels, respectively. In fact, blue derivatives of GFP actually have an extended emission 'tail' which bleeds into the green channel. This problem also occurs with other well known fluorophores. Although fluorescein appears bright green to the eye, it has a substantial red tail that bleeds into the rhodamine channel in double-label experiments. A FRET

(fluorescence resonance energy transfer) deconvolution, based on a three-channel analysis from conventional epifluorescence cubes, will be discussed in a future publication.

FIMS technology is essential for addressing inherently difficult problems which arise when one is attempting to measure the relative concentrations of GFP variants in microscopic samples. Relatively speaking, spectrally separating combinatorial organic fluorophores, such as those used in chromosome painting, is a much simpler task than separating the spectra of fluorescent proteins. This is because the protein engineering likely to be needed to create numerous spectrally-distinct GFP derivatives is not as straightforward as the organic chemistry that has produced the current catalogue of organic fluorophores (Haugland, 1994). In other words, we will not have the luxury of a long list of GFP derivatives, fully separable by conventional filter cubes. Even for relatively simple organic dye-labeling experiments, such as those used in comparative genomic hybridization (CGH), the ability to effectively separate the fluorescence contributions from the various fluorophores and accurately measure the intensity of their fluorescence emission is crucial (Kallioniemi et al., 1992; du Manoir, 1995).

Epifluorescence Cubes. The dichroic mirror in an epifluorescence microscope has several important functions, including: (1) illumination and light collection (both through the objective), and (2) discrimination of excitation and emission wavelengths (supplementing the optical filters). The dichroic properties of the mirror are essential for reflecting the shorter wavelengths of light down to the sample for excitation, while transmitting longer wavelengths up to the detector. In standard commercial cubes (Fig. 2a), the dichroic mirror 'cuts on' optical transmission at a wavelength intermediate between the excitation filter and the emission filter.

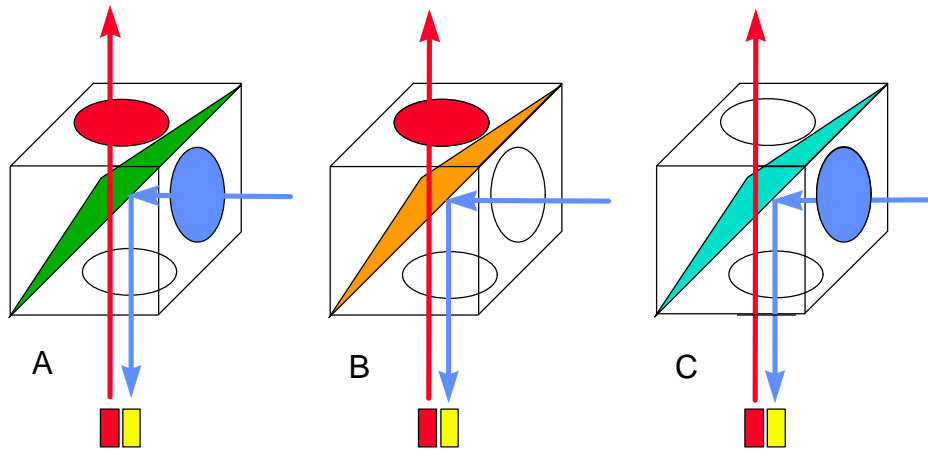


Fig. 2. Three different optical cubes for: (A) a standard epifluorescence microscope, (B) FIMS excitation scans, and (C) FIMS emission scans. Details of the ray tracing are described in the text.

The microscope turret of the FIMS prototype holds two ‘cubes’, one optimized for excitation scans and the other for emission scans (Figs. 2*b* and 2*c*, respectively). Both cubes utilize a dichroic mirror; however, the excitation cube lacks an excitation filter and the emission cube lacks an emission filter. In place of these filters, FIMS uses a fiber-optically linked scanning monochromator for excitation and a circular variable interference filter (CVIF) for emission. The dichroic mirror of the emission cube is designed to cut-on within 10 nm to the red of the monochromator’s narrow band excitation, while the dichroic mirror of the excitation cube cuts-on at a wavelength just to the blue of the selected emission wavelength. It is also possible to remove both filters and use the monochromator to select the excitation wavelengths and the CVIF to selectively block the emitted light.

The dichroic mirror was chosen such that it cannot interfere with the scan, a problem which is not a concern in a conventional fixed-wavelength epifluorescence microscope. In Fig. 2, ray tracings for all three cubes show the interaction of light with a hypothetical yellow fluorophore which absorbs a blue photon and fluoresces in the red. In the standard cube, the blue photon passes through the excitation bandpass filter (right side of the cube) and is reflected downward through the objective to the sample by the dichroic mirror via an open port (bottom side). The returning fluorescence (red) photon traverses the bottom port, the dichroic mirror, and the red bandpass filter (top). In the standard cube, both the dichroic mirror and the emission filter block the exciting light. Schematically, the dichroic mirror is colored green to depict a transmission cut-on in the green, which reflects the blue excitation downward and transmits the red emission upward. FIMS configurations of epi-cubes that are used for fluorescence excitation and emission scans are depicted in Figs. 2*b* and 2*c*, respectively. The dichroic mirror in the excitation cube (orange cut-on) is designed to block a greater range of wavelengths, extending from the blue to just short of the observational wavelength, in order to efficiently reflect the exciting light during a scan. In contrast, the dichroic mirror in cube C (cyan cut-on) accommodates a wide range of fluorescence emission wavelengths.

Utilization of the CVIF. For the blocking filter in fluorescence emission scans, FIMS uses a circular variable interference filter (CVIF, Fig. 3) positioned directly above the projection eyepiece (PE). This configuration places the filter at a position in space where the projection optics are transmitting nearly collimated light within the narrowest waist (spot size). Both the solid angle of light from the projection eyepiece to the CCD array and the spot size have been exaggerated in Fig. 3. These parameters have been measured in the current instrument as 10 degrees and 0.5 millimeters, respectively. By taking into consideration the physical size and ‘ramp’ of the CVIF, along with known equations for spectral broadening of Fabry-Perot filters with a solid cone of light (Macleod, 1986), one can calculate that this configuration has the ability to tune at 2 nm resolution. Broader bandpass (i.e., more light and less spectral differentiation) can be obtained by moving the filter slightly off the narrowest waist along the z-axis.

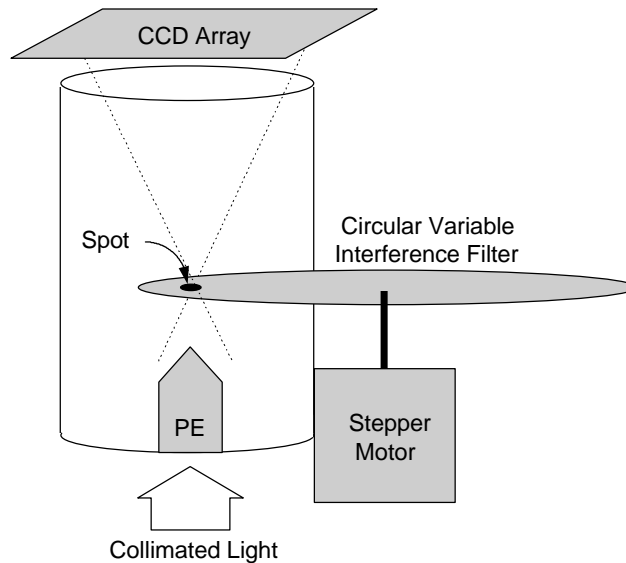


Fig. 3. Schematic diagram showing the placement of the circular variable interference filter (CVIF) at the narrowest waist. In FIMS, a CVIF replaces the fixed-wavelength emission filter of a commercial epifluorescence microscope, and is selectively tunable to a wide range of wavelengths (400–720 nm). In the prototype FIMS instrument, the CVIF was positioned manually by a vernier that was pin-registered to the radial position of the filter. PE: projection eyepiece.

Materials and Methods

Hardware. FIMS is currently based on an Olympus BX60 microscope, an upright epifluorescence optical bench which also supports brightfield work. FIMS spectra have been acquired using 10×, 20×, 40×, and 100× objectives. In the prototype of FIMS, excitation measurements used a 1.5 m quartz fiber optic coupled to the light source of an existing PTI fluorimeter via the fluorimeter sample compartment. The fiber optic coupling to the microscope was optimized through an aspheric condenser lens attachment. A CVIF, selectively tunable through the wavelength range of 400–720 nm, was mounted within the manufacturer's pin-registered optical housing. A relay optics tube (holding the projection eyepiece and the reduction lens) was machined with a mill in order to position this housing at the narrowest waist. In this prototype, wavelength selection requires manual rotation of the CVIF according to a vernier and an equation related to the method by which the thin layer interference filter was formed: $\lambda = (540 - 2\theta)$ in nm. FIMS uses two dichroic mirrors which either cut-on transmission just to the blue of the emission wavelength (for excitation scans) or just to the red of the excitation wavelength (for emission scans). We have been using the unmodified turret of the BX60 to house these beamsplitters within conventional epifluorescence cubes. A KAIROS K7 CCD camera was used to acquire all data stacks. The KAIROS K7 CCD camera (16 bit, 760 × 510 resolution) was coupled to the microscope using customized relay optics in order to facilitate placement of the CVIF (Yen, 1982) in the optical path between the projection eyepiece and the detector. The K7 CCD chip was coated for enhanced blue sensitivity and Peltier cooled to 4° C. Light-minus-dark images (1 s exposure) were downloaded through the parallel port of a personal computer and processed by software written in-house.

Software. Source code was developed under Microsoft Visual C++ using the Microsoft Foundation Classes; approximately 100,000 lines of (*HyperDIS*) code was written per industry standards, which is Win95 compliant. *HyperDIS* software development will be discussed in a future publication.

Calibration. Radiometric calibration of the FIMS instrument was achieved by sequentially operating on the raw data using several software programs. In determining instrument response, we took into account contributions from the light source, monochromator, CVIF and camera. The strongest contributors to the response function are the diffraction grating of the monochromator and the coated CCD detector. The throughput of the grating falls off linearly on either side of the blaze (500 nm), and the K7 CCD camera is less sensitive in the blue than in the red. Xenon light sources are fairly uniform in intensity throughout the wavelength range used in these studies, with the exception of a few weak lines to the blue of the grating's blaze. The CVIF has a relatively flat percent transmission (~50% T) throughout its operative range (400 - 720 nm), due to the fact that it was fabricated in a single evaporator run on a single substrate - unlike conventional emission filters in typical epifluorescence cubes, which vary significantly from filter to filter. Response functions were derived using *Mathematica* (Wolfram, 1991) to fit empirical data obtained from the light source and detector; both as a function of wavelength. For the instrument configuration described here, the calibration functions listed below are used for excitation and emission, where λ is the wavelength being scanned. The radiometrically calibrated fluorescence intensity is calculated by normalizing the CCD grayvalue by the value of the corresponding calibration function at that wavelength.

Calibration functions for excitation scans are:

$$X(\lambda) = 1810 + 5.66\lambda \quad (\lambda < 470 \text{ nm})$$

$$X(\lambda) = 1500 - 1.40\lambda \quad (\lambda \geq 470 \text{ nm})$$

The calibration function for emission scans is:

$$M(\lambda) = 574 - 3.50\lambda + .00694\lambda^2 - 0.00000432\lambda^3 + 19.3 \exp[-0.0003(\lambda - 560)^2]$$

GFP Samples. GFP mutants having fluorescence excitation and emission maxima that are red-shifted relative to wild-type GFP were expressed in *E. coli* strain BL21 (DE3). RSGFP8 (Lossau *et al.*, 1996) contains the mutations F64L and S65T, which move the excitation / emission maxima from 403/508 nm (in wild-type) to 489/515 nm. MutY2 contains the mutations F64L, S65T and T203Y, which move the fluorescence excitation/emission maxima to 510/524 nm. RSGFP8 is identical to the F64L+S65T mutant isolated independently by Cormack *et al.*, (1996), and its spectral properties are similar to the Ser-65 mutants isolated by Delagrave *et al.* (1995). The MutY2 phenotype is similar to that of the previously reported point mutants T203Y and T203H, which also have red-shifted excitation and emission maxima (Ormö *et al.*, 1996).

Fluorescent Beads. A collection of polystyrene latex beads (FluoSpheres; 1 μm diameter), in which each member of the set is labeled with one to six different (energy coupled)

fluorescent dyes, was obtained from Molecular Probes (Eugene, OR). The beads have emission maxima at 515, 560, 605, 645, 685 and 720 nm.

Results

Fluorescence Emission Spectra. As a stable test target, FIMS emission spectra were acquired on an equi-unit mixture of six different types of 1 μm diameter fluorescent beads (FluoSpheres, Molecular Probes). Stock beads from the manufacturer with emission maxima at 515, 560, 605, 645, 685 and 720 nm were mixed, diluted 100-fold, spread over $\sim 1\text{ cm}^2$ area on a glass slide, and air dried. All beads were imaged through a cube lacking a blocking filter, but including a 480 nm excitation bandpass filter and a 505 nm dichroic mirror. The blocking filter was replaced by the circular variable interference filter at the narrowest waist of the projection eyepiece. A 50W tungsten light source was used directly. The optical path included a 40 \times objective, a 2.5 \times projection eyepiece, and a 0.8 \times reduction lens.

Hyperspectral pseudocoloring of this image stack utilized KAIROS *HyperDIS* software and involved the following steps: (1) radiometric calibration and rescaling of each image in the stack according to excitation and emission responses, (2) identification of background pixels by forming a list of 'category 0' pixels which fall within a narrow range of intensity values or below a certain threshold value, (3) sorting of all pixels according to the wavelength of maximum emission, (4) graphic display of such spectra on a color contour plot, (5) interactive selection of rows (i.e., spectra) within the contour plot, (6) calculation of a mean spectrum for each category, (7) binning of all pixels within the image into one of the spectral categories, and (8) selection of colors from a palette for encoding each spectral category. As a result of this process, the 515, 560, 605, 645, 685 and 720 nm beads displayed in Fig. 4 have been painted blue, green, yellow, orange, red and white, respectively. The accuracy of the FIMS hyperspectral image representation was verified by comparing the image shown in Fig. 4 with monochrome images from selected wavelengths, as well as by recalling single pixel spectra (Fig. 6) for each bead. The differences in peak height are consistent with conventional (single cuvette) fluorimetry, and are due to variable dye loading of the beads and sequential fluorescence energy transfer from shorter to longer wavelengths; e.g., the 720 nm bead emits fluorescence as a result of 5 sequential energy transfer steps from the other 5 dyes.

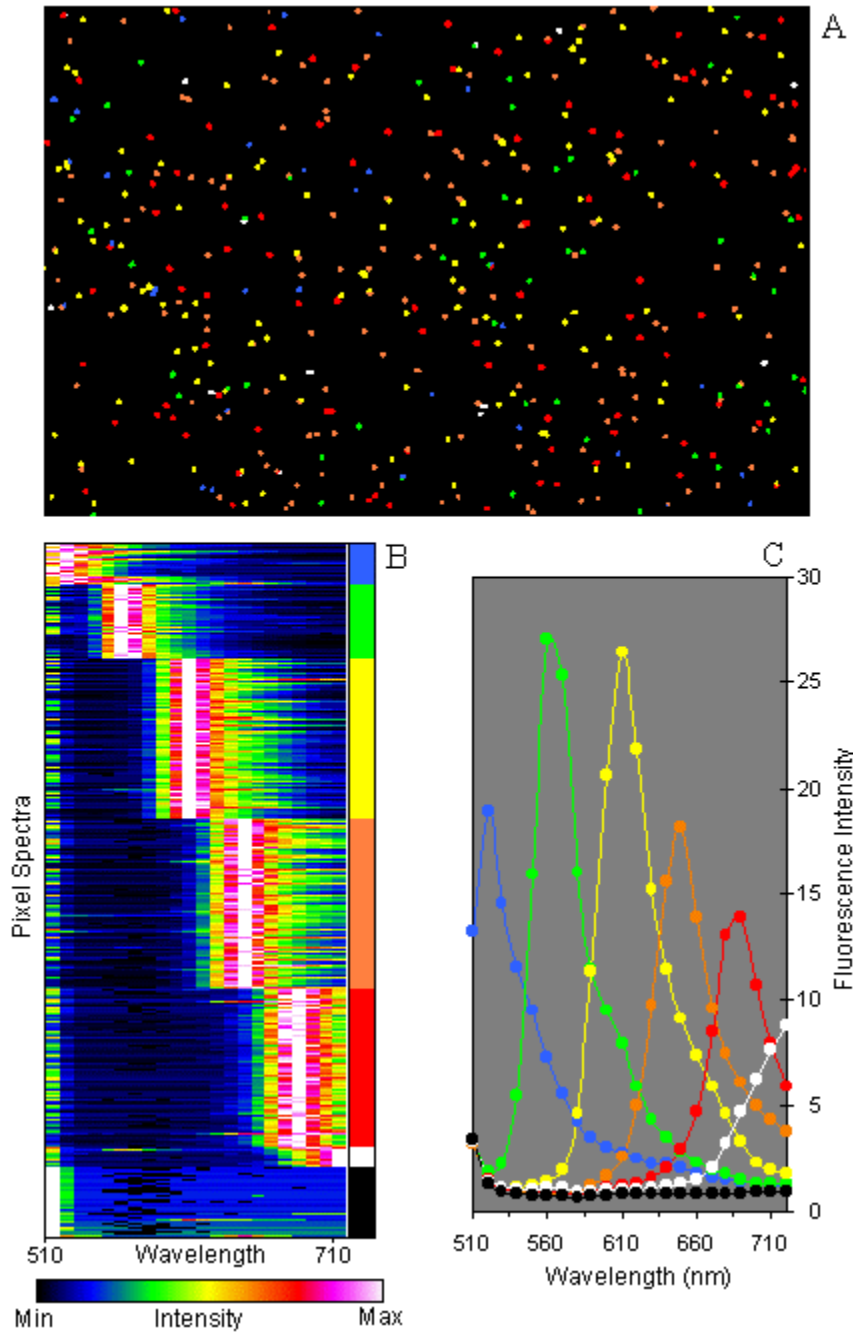


Fig. 4. FIMS analysis of a mixture of 6 different fluorescent beads. Panel A uses hyperspectral pseudocoloring techniques to display each category of beads as a different color. This color code is consistent with the vertical bar to the right of the contour plot in Panel B, which shows (desampled) single pixel emission spectra intensity as a function of wavelength. The color coding is also maintained in Panel C in which the average spectrum for the 6 types of beads plus background (pseudocolored black) are plotted.

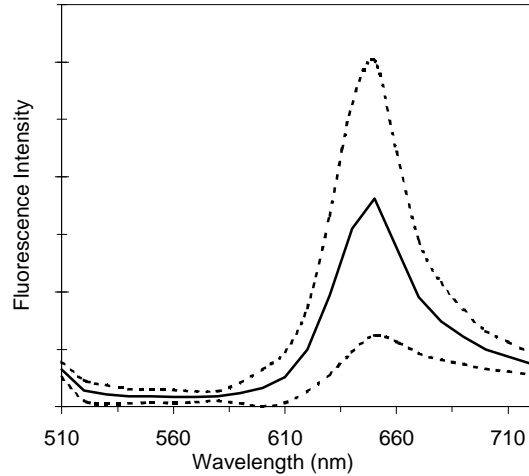


Fig. 5. Statistics of the spectra acquired for the 645 nm bead type that was pseudocolored 'orange'. The average spectrum is given by the solid line. The dotted lines represent this spectrum ± 1 standard deviation. The distribution in peak heights is due to differential dye loading of the beads and the inclusion of edge pixels. During hyperspectral painting, these data are displayed during run-time, so that the user is able to see whether different spectral classes are being properly segregated.

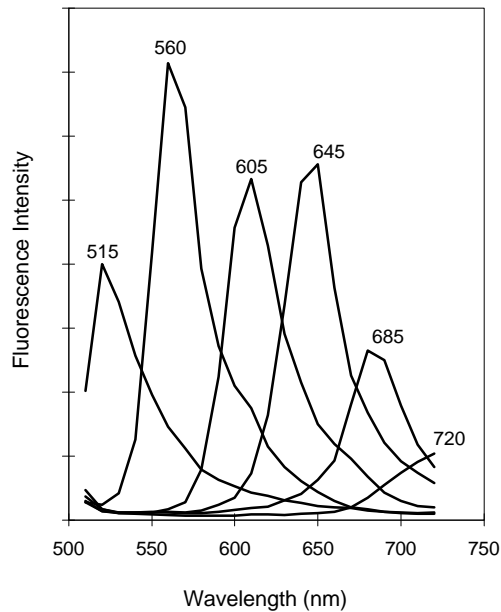


Fig. 6. Single pixel spectra from *HyperDIS* displayed during run-time as the user interacts with the image window or contour plot (such as in Fig. 4, Panels A and B) via the mouse.

Fluorescence Excitation Spectra. For the fluorescence excitation test target, a mixture of three different strains of *E. coli* expressing wild-type and two genetic variants of GFP

(RSGFP8 and MutY2) was used (Delagrave *et al.*, 1995; Lossau *et al.*, 1996; Cormack *et al.*, 1996). Conventional fluorimetry of proteins purified from these three strains are shown in Fig. 7. For imaging spectroscopy, equal volumes of bacteria were mixed together, concentrated by centrifugation (10-fold), stirred into 3% aqueous low melt agarose on a warm slide, and compressed by a cover slip with manual pressure. All bacteria were imaged through a modified cube lacking an excitation filter (i.e., 515 nm longpass emission filter with a 505 nm dichroic mirror). The excitation filter and tungsten light source were replaced by a fiber-optically coupled (quartz) 75 W Xe source whose output was diffracted through a ¼ meter monochromator (PTI, 500 nm blaze, 5 nm bandpass). The optical path included a 100× oil objective, a 2.5× projection eyepiece, and a 0.8× reduction lens. A total of 31 images were captured by a KAIROS K7 CCD camera which is Peltier cooled to 4°C, with 1 s light-minus-dark frames. Hyperspectral pseudocoloring of this excitation image stack (Fig. 8) utilized *HyperDIS* software similar to the procedure used for the emission stack.

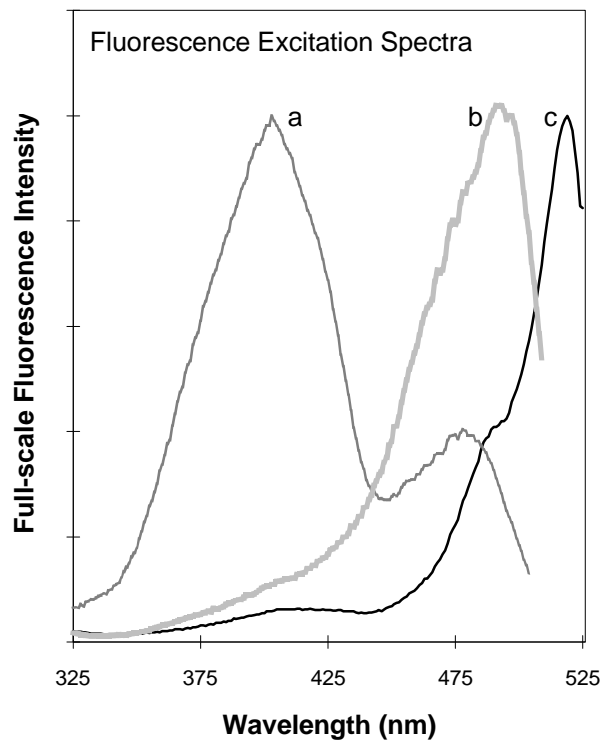


Fig. 7. Conventional fluorescence excitation spectra of purified protein samples from three *E. coli* strains expressing wild-type GFP and two mutants: (a) wild-type GFP, (b) RSGFP8, (c) MutY2. These three variants have fluorescence excitation maxima at 403, 489, and 510 nm, respectively. MutY2 was recently isolated by combinatorial mutagenesis; it emits 15 nm to the red of wild-type. Emission was detected 20 nm to the red of the ending data point for each scan.

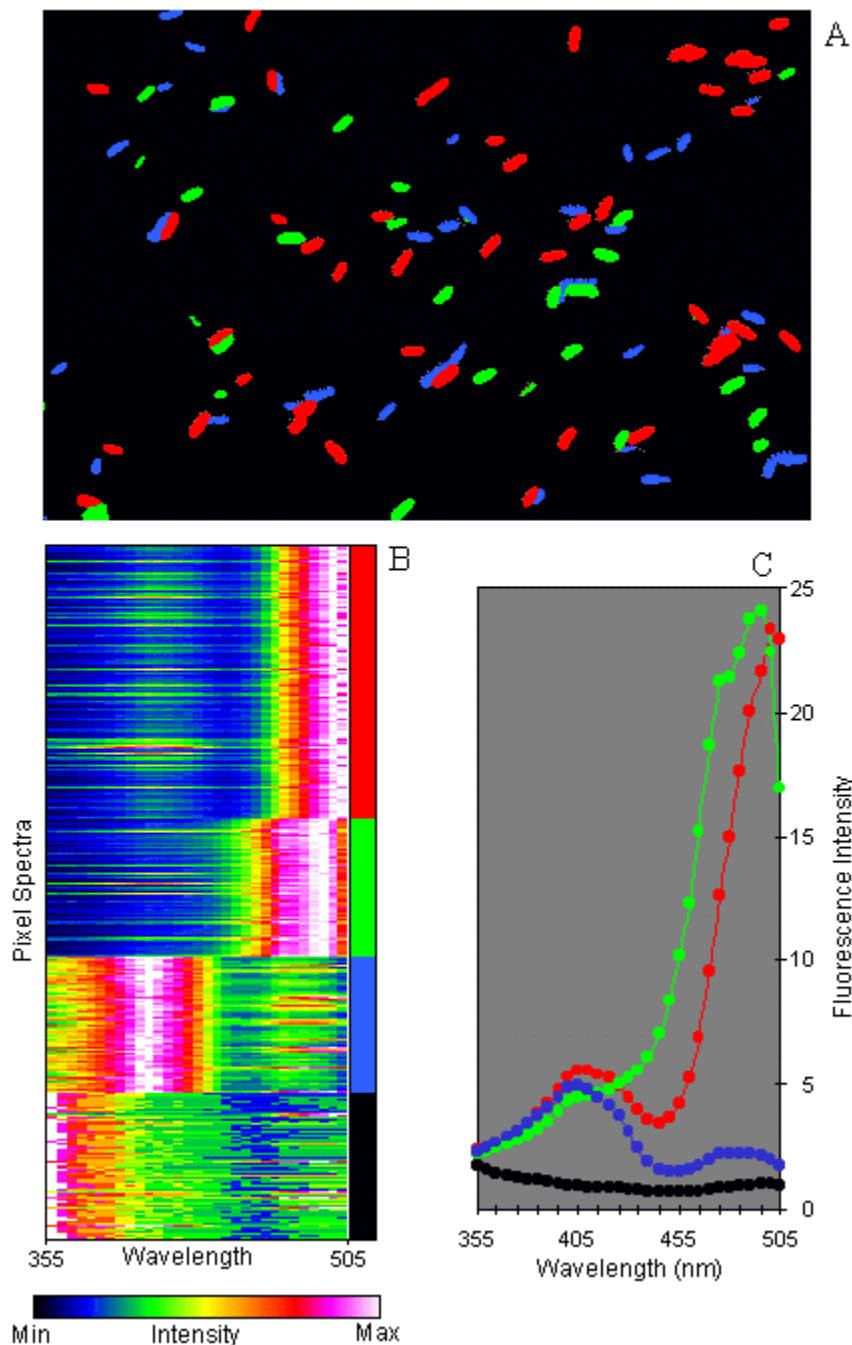


Fig. 8. FIMS analysis of a mixture of 3 different strains of *E. coli* expressing wild-type GFP and two mutants (pseudocolored): Wild-type (blue), RSGFP8 (green), and MutY2 (red). Conventional fluorimetry data from these strains are plotted in Fig. 7. Very similar to Fig. 4, Panel A uses hyperspectral pseudocoloring techniques to display each *E. coli* bacterium as a different color, based on its wavelength of maximum excitation. This color code is consistent with the vertical bar to the right of the contour plot in Panel B which shows (desampled) single pixel excitation spectra intensity as a function of wavelength. The color coding is also maintained in Panel C, which shows the average spectra for the 3 types of GFP-expressing bacteria. Background is pseudocolored black.

Discussion

Cell biologists are becoming more familiar with microscopes that can resolve spectral information (in addition to spatial information) because an increasing number of fluorophores have overlapping excitation and emission spectra. Fluorescence *in situ* hybridization (FISH) experiments (Schröck *et al.*, 1996; Speicher *et al.*, 1996) have recently employed combinatorial fluorescent dyes to produce uniquely 'colored' chromosomes for karyotyping. In early experiments, such chromosome painting relied on interference microscopy. By using a triple bandpass filter to obtain 2-D interferograms, 'interference stacks' were phase corrected and then Fourier transformed to obtain spectral and spatial information. However, with a triple bandpass filter in place, emission scans are limited to three narrow transmissive windows, which preclude single pixel fluorescence emission scans throughout most of the visible spectrum. Since the excitation light is not within the interferometer's path, excitation scans are not possible; nor can absorption scans be acquired.

In contrast to interferometry techniques, FIMS produces radiometrically calibrated image stacks, in which each image is restricted to a single wavelength that requires no further processing for viewing. From this FIMS stack, we have obtained both excitation and emission spectra at single pixel resolution with a quality rivaling that of a conventional fluorimeter. In a future publication, a *High Resolution Imaging Microscope* (HIRIM) will be shown to produce absorption spectra comparable in quality to a conventional spectrophotometer.

One of the unique and essential elements of FIMS technology is the utilization of physically robust CVIFs with outstanding spectral characteristics. These 'wedge' interference filters are constructed by evaporating dielectric materials onto a single glass substrate, a process which produces a device having highly parallel surfaces (important for image registration) and optical uniformity with respect to changes in the percentage transmission of the filter (facilitating radiometric calibration). Alternative filter devices which could be used for imaging spectroscopy include acousto-optical tunable filters (AOTF) (Kurtz *et al.*, 1987) and electro-polarization devices such as liquid crystal tunable filters (LCTF) (Morris *et al.*, 1994; Wang & Lewis, 1996). We have rejected these designs due to their poor acceptance angles, limited wavelength range, and high cost, as well as their potential for degrading the image.

Although many epifluorescence imaging microscopes are considered "multi-spectral" (due to their use of multiple epifluorescence cubes), they nevertheless suffer from the problem that their blocking filter surfaces are often not parallel; consequently, as images are acquired at various wavelengths through different cubes, image registration problems arise which may be more complicated than simple translation of the image (Bright, *et al.*, 1989; Jericevic *et al.*, 1989; Waggoner *et al.*, 1989; Fricker & White, 1992). Replacing the CVIF with a filter wheel is also not desirable from an engineering standpoint because each of the interference filters is likely to have been fabricated in a different evaporator run; therefore, the percent transmission will vary from filter to filter. This creates abrupt changes in grayscale between adjacent images in the stack, which in turn requires extensive calibration of each filter set. With a single CVIF blocking filter, we see only smooth monotonic variation in the %T, requiring only minimal adjustment for accurate calibration.

Summary

The main performance features of the current FIMS prototype instrument can be summarized as follows:

- Processing of ~100,000 single-pixel fluorescence spectra per hyperspectral stack
- Radiometric calibration for both excitation and emission scans
- Rapid processing of single-pixel fluorescence spectra into categories
- Run-time display of single-pixel fluorescence spectra
- Run-time display of the mean and standard deviation of all spectral categories
- Hyperspectral pseudocoloring of images based on spectral categories

As well as hardware development to fully automate the FIMS instrument, future work will include enhanced software for 'pixel purification' and spectral deconvolution.

Acknowledgments

FIMS hardware and software development was supported by NIH 1R43GM55085 and KAIROS IR&D funds. Related work on protein engineering and GFP photochemistry is supported by NIH R01GM42645, 2R44GM53287, and DOE DE-FG03-96ER20211. FIMS is patent pending.

References

- Arndt-Jovin, D.J. & Jovin, T.M. (1989) In: *Cell Structure and Function by Microspectrofluorometry* (Kohen, E. & Hirschberg, J.G., eds.) pp. 417–448, Academic Press, San Diego.
- Bright, G.R., Fisher, G.W., Rogowska, J. & Taylor, D.L. (1989) *Methods Cell. Biol.* **30**:157–192.
- Chalfie, M., Tu, Y., Euskirchen, G., Ward, W. W. & Prasher, D.C. (1994) *Science* **263**:802–805.
- Cormack, B. P., Valdivia, R. H. & Falkow, S. (1996) *Gene* **173**:33–38.
- Delagrave, S., Hawtin, R.E., Silva, C.M., Yang, M.M. & Youvan, D.C. (1995) *Bio/Technology* **13**:151–154.
- Doyle, T. & Botstein, D. (1996) *Proc. Natl. Acad. Sci. U.S.A.* **93**:3886–3891.
- du Manoir, S., Scrock, E., Bentz, M., Speicher, M.R., Joos, S., Ried, T., Lichter, P. & Cremer, T. (1995) *Cytometry* **19**:27–41.
- Fricke, M.D. & White, N.S. (1992) *J. Microsc.* **166**:29–42.
- Haugland, R.P. (1994) *Methods Cell Biol.* **42**:641–663.

Hirschberg, J. G., Wouters, A.W., Kohn, E., Kohen, C., Thorell, B., Eisenberg, B., Salmon, J.M. & Ploem, H.S. (1979) In: *Multichannel Image Detectors*, (Talmi, Y., ed.) pp. 263–289, American Chemical Society, Washington, D.C.

Htun, H., Barsony, J., Renyi, I., Gould, D. L. & Hager, G. L. (1996) *Proc. Natl. Acad. Sci. U.S.A.* **93**:4845–4850.

Jericevic, Z., Wiese, B., Bryan, J.B. & Smith, L.C. (1989) *Methods Cell Biol.* **30**:47–83.

Kallioniemi, A., Kallioniemi, O.-P., Sudar, D., Rutovitz, D., Gray, J.W., Waldman, F. & Pinkel, D. (1992) *Science* **258**:818–821.

Kasten, F.H. (1989) In: *Cell Structure and Function by Microspectrofluorometry* (Kohen, E. & Hirschberg, J.G., eds.) pp. 3–50, Academic Press, San Diego.

Kohen, E., Thorell, B., Hirschberg, J.G., Wouters, A.W., Kohen, C., Bartick, P., Salmon, J.-M., Viallet, P., Schachtschabel, D.O., Rabinovitch, A., Mintz, D., Meda, P., Westerhoff, H., Nestor, J. & Ploem, J.S. (1981) In: *Modern Fluorescence Spectroscopy* (Wehry, E.L., ed.) pp. 295–346, Plenum Press, New York.

Kurtz, I., Dwelle, R. & Katzkaq, P. (1987) *Rev. Sci. Instrum.* **58**:1996–2003.

Lossau, H., Kummer, A., Heinecke, R., Pöllinger-Dammer, F., Kompa, C., Bieser, G., Jonsson, T., Silva, C.M., Yang, M.M., Youvan, D.C. & Michel-Beyerle, M.E. (1996) *Chem. Phys.* **213**:1-16.

Macleod, H.A. (1996) *Thin-Film Optical Filters*, Macmillan Publishing, New York.

Morris, H.R., Hoyt, C.C. & Treado, P.J. (1994) *Appl. Spectr.* **48**:857–866.

Ormö, M., Cubitt, A.B., Kallio, K., Gross, L.A., Tsien, R.Y. & Remington, S.J. (1996) *Science* **273**:1392–1395.

Plautz, J.D., Day, R.N., Dailey, G.M., Welsh, S.B., Hall, J.C., Halpain, S. & Kay, S. A.. (1996) *Gene* **173**: 83–87.

Ploem, J.S. (1989) In: *Cell Structure and Function by Microspectrofluorometry* (Kohen, E. & Hirschberg, J.G., eds.) pp. 119–130, Academic Press, San Diego.

Ruch, F. & Leemann, U. (1973) In: *Micromethods in Molecular Biology* (Neuhoff, V., ed.) pp. 329–346, Springer-Verlag, Berlin.

Schröck, E., du Manoir, S., Veldman, T., Schoell, B., Weinberg, J., Ferguson-Smith, M.A., Ning, Y., Ledbetter, D.H., Bar-Am, I., Soenksen, D., Garini, Y. & Ried, T. (1996) *Science* **273**:494–497.

Speicher, M.R., Ballard, S.G. & Ward, D.C. (1996) *Nature Genet.* **12**:368.

Vane, G., Duval, J.E. & Wellman, J.B. (1993) In: *Remote Geochemical Analysis: Elemental and Mineralogical Composition* (Pieters, C. M. & Englert, P.A..J., eds.) Cambridge University Press, New York.

Waggoner, A., DeBasio, R., Conrad, P., Bright, G.R., Ernst, L., Ryan, K., Nederlof, M. & Taylor, D. (1989) *Methods Cell Biol.* **30**:449–478.

Wang, X.F. & Herman, B. (1996) *Fluorescence Imaging Spectroscopy and Microscopy*. John Wiley & Sons, New York.

Wang, X. & Lewis, E.N. (1996) In: *Fluorescence Imaging Spectroscopy and Microscopy* (Wang, X.F. & Herman, B., eds.) pp. 125–156, John Wiley & Sons, New York.

Wolfram, S. (1991) *Mathematica*, Addison-Wesley Publishing, New York.

Yang, T., Kain, S., Kitts, P., Kondepudi, A., Yang, M.M. & Youvan, D.C. (1996) *Gene* **173**:19–23.

Yen, V. L. (1982) *Optical Spectra*, OCLI, Santa Rosa, California.

Yokoe, H. & Meyer, T. (1996) *Nature Biotechnology* **14**:1252–1256.

Youvan, D.C. (1994) *Nature* **369**: 79–80.

Youvan, D.C., Goldman, E., Delagrave, S. & Yang, M.M. (1994) *Methods Enzymol.* **246**:732–748.